An Efficient Alternative to Compute the Genus of Binary Volume Models

Irving Cruz-Matías and Dolors Ayala
Department de Llenguatges i Sistemes Informàtics, Universitat Politècnica de Catalunya, Barcelona, Spain

Keywords: Binary Volume Models, Orthogonal Polyhedra, Euler Characteristic, Euler Number or Genus.

Abstract: In this paper we present a method to compute the Euler characteristic (χ) and the genus of a volume dataset. It uses an alternative decomposition model to represent binary volume datasets: the Compact Union of Disjoint Boxes (CUDB). The method is derived from the classical method used with a voxel model and the computation of χ and the genus is achieved by analyzing the connectivity among boxes and using a CUDB connected-component labeling process. We have tested our method both with phantom and real datasets and we show that it is more efficient than previous methods based on the voxel model, and other alternative models.

1 INTRODUCTION

The measurement of the topological characteristics of an object such as its number of connected components and cavities or its genus is a useful tool in many applications. For instance, the genus is related to the connectivity and is used to measure the strength of bones (osteoporosis) or the quality of the biomaterials designed to repair them.

The main contribution of this paper is a method to compute the Euler characteristic, χ, and the genus of binary volume datasets as well as of pseudo-manifold orthogonal polyhedra (OP) without voxelizing them, or converting them to a homotopic manifold analog. The binary volume dataset is represented with an alternative model, the Compact Union of Disjoint Boxes (CUDB). The computation of χ is achieved by counting the number of unitary basic elements (voxels, surfels, linear elements an points) with which a box of the CUDB model contributes, and taking into a count the overlapping regions among boxes. Then, to obtain the genus, we previously computed the number of connected components and cavities of the object by applying a connected-component labeling (CCL)-based method to the CUDB model of both the object and its complement.

We have tested several phantom models and real datasets and compared the results and performance of our method with those that compute the same parameters using the voxel model and another alternative model.

2 BACKGROUND AND RELATED WORK

A binary volume model is a union of voxels with values restricted to 0 (background) and 1 (foreground). Foreground voxels correspond to the interior of the object and background voxels the exterior. Three kinds of adjacency relations are defined between voxels: 6, 18 and 26-adjacency. Two voxels are 6-adjacent if they share a face, 18-adjacent if they share an edge or a face, and 26-adjacent if they share at least a vertex (see Figure 1). An adjacency pair (m, n) defines the adjacency of a binary volume dataset, meaning that the foreground is m-adjacent and background is n-adjacent. Using some adjacency pairs leads to paradoxes making the choice of foreground and background to become critical, and several times it is not clear what is the foreground and what is the background (Kong and Rosenfeld, 1989; Latecki et al., 1995). Therefore proper adjacency pairs that avoid paradoxes are useful and in 3D these adjacency pairs are (6, 26), (26, 6) (Lachaud and Montanvert, 2000).

A binary volume model is manifold (well-composed) if it lacks the shapes shown in Figure 2 (left and middle), modulo reflections and rotations (Latecki, 1997). However, general binary volumes with adjacency pair (6, 26) or (26, 6) are non-manifold as 26-adjacency allows non-manifold shapes. The Euler characteristic, χ, can be computed from a voxel model with the following expression (Odgaard and Gundersen, 1993):

Cruz-Matías I. and Ayala D..
An Efficient Alternative to Compute the Genus of Binary Volume Models.
DOI: 10.5220/0004280000180026
In *Proceedings of the International Conference on Computer Graphics Theory and Applications and International Conference on Information Visualization Theory and Applications* (GRAPP-2013), pages 18-26
ISBN: 978-989-8565-46-4

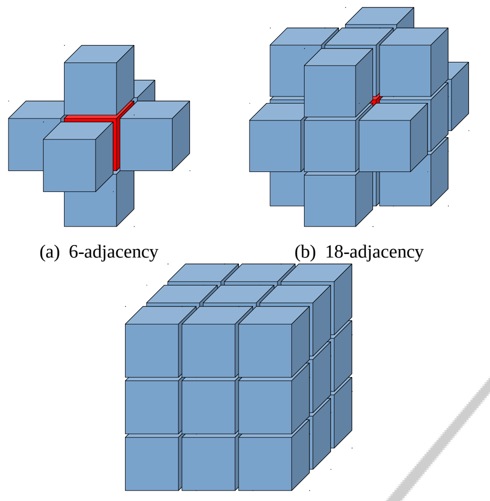

(a) 6-adjacency (b) 18-adjacency

(c) 26-adjacency

Figure 1: Kinds of adjacency of a voxel with its local neighborhood.

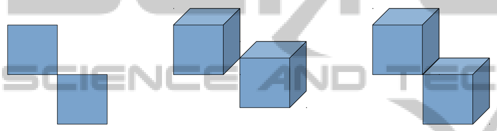

Figure 2: Non-manifold 2D (left) and 3D (middle and right) configurations.

$$\chi = n_0 - n_1 + n_2 - n_3 \tag{1}$$

where n_0, n_1, n_2 and n_3 are, respectively, the number of vertices (points), edges (linear elements), faces (surfels) and voxels of the voxel model. This expression can be applied to several adjacency pairs (Toriwaki and Yonekura, 2002). In the solid modeling field, χ can also be computed from a polyhedron using the following expression (Mantyla, 1988):

$$\chi = V - E + F - R \tag{2}$$

where V, E, F and R are, respectively, the number of vertices, edges, faces and internal rings of faces. This expression can also be applied to triangular surfaces, F being the number of triangles and $R = 0$. From the theory of homology, the Euler-Poincaré formula relates χ with the Betti numbers h_i (Massey, 1991):

$$\chi = h_0 - h_1 + h_2 \tag{3}$$

where h_0, h_1 and h_2 are, respectively, the number of connected components, the connectivity and the number of isolated cavities. h_0 and h_2 are usually computed using CCL-based methods over voxels, polyhedron faces or triangles, depending on the model used. Then, the connectivity h_1 which is related to the genus, can be computed from χ, h_0 and h_2 using Expression 3.

Although binary volumes with adjacency pairs (6, 26) or (26, 6) are non-manifold, χ and the genus can be computed unambiguously for them. When computing n_0 and n_1 in Expression 1 the adjacency pair is taken into consideration in such a way that non-manifold edges and vertices are counted once for 26-adjacency and twice for 6-adjacency. For example, in the case of the object depicted in Figure 3, considering the adjacency pair (26, 6), the number of connected components (h_0) is 1 and vertices v_1 to v_6 and edges e_1, e_2 are counted just once because they belong to two connected voxels, so, the genus (h_1), which can be seen as the number of handles, is 2. But considering the adjacency pair (6, 26), $h_0 = 3$ and in this case the vertices v_1 to v_6 and edges e_1, e_2 must be counting twice because they belong to separating two voxels, giving a genus=0.

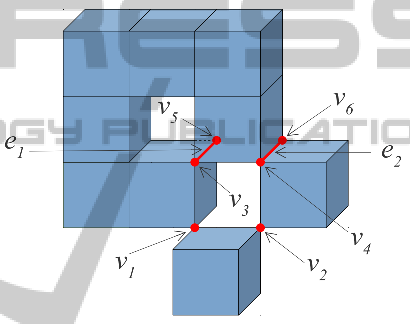

Figure 3: Illustrative figure consisting of 9 voxels for calculating the genus depending on the selected adjacency pair.

A binary volume dataset can be represented in a compact way by an OP (Khachan et al., 2000). Based on this fact, a previous approach (Ayala et al., 2012) computes χ and the genus of a binary volume dataset using expression 2. In this method, the binary volume dataset is represented with a model suitable for OP and when the object presents non-manifold configurations, it needs to be converted into an homotopic manifold analog. This approach has proved to be more efficient than methods based on voxel models and triangle meshes.

Expression 2 and 3 are used to compute the connectivity of a triangular mesh representing some adenine properties in the biochemistry field (Konkle et al., 2003). In isosurface extraction, the topology-preservation is sometimes a desirable property that can be evaluated by computing χ (Schaefer et al., 2007). In the Bio-CAD field, the connectivity is related to biomechanical properties and is used to measure the strength of bone or other materials. The method based on Expressions 1 and 3 is used to evaluate the osteoporosis degree of mice femur (Martín-Badosa et al., 2003) or human vertebrae (Odgaard and Gundersen, 1993) or to evaluate hydraulic properties of sintered glass (Vogel et al., 2005).

Binary volume models are mostly represented with the classical voxel model. However, for specific purposes, several alternative models have been devised. Hierarchical decomposition models as octrees and kd-trees have been used for Boolean operations (Samet, 1990), CCL (Dillencourt et al., 1992) and isosurface extraction (Andújar et al., 2002; Vanderhyde and Szymczak, 2008). Other models store only surface voxels to improve spatial or querying performance, such as the semi-boundary (Grevera et al., 2000) and the slice-based binary shell representation (Kim et al., 2001).

In this work we represent a binary volume with a decomposition model, the Compact Union of Disjoint Boxes (CUDB). This model is suitable for binary volumes as well as for OP and is introduced in the next section. Section 4 presents our approach to compute χ and the genus of a binary volume. The first contribution is a method to compute χ, that applies Expression 1 to each box of the CUDB, taking into account the overlapping regions among boxes. The second contribution is a CCL-based method that obtains the connected components and cavities of the object in order to compute the connectivity from Expression 3. Section 5 presents the results obtained with several phantom and real datasets, besides, we also compare the performance of our method with the methods based respectively on the voxel model (Toriwaki and Yonekura, 2002) and on OP (Ayala et al., 2012). Finally, Section 6 concludes this paper.

3 THE CUDB MODEL

To introduce the Compact Union of Disjoint Boxes (CUDB) model, we will consider the pseudo-manifold orthogonal polyhedron (OP) that constitutes the continuous analog of the binary voxel model.

Let P be an OP and Π_c a plane whose normal is parallel, without loss of generality, to the X axis, intersecting it at $x = c$, where c ranges from $-\infty$ to $+\infty$. Then, this plane sweeps the whole space as c varies within its range, intersecting P at certain intervals. Let us assume that this intersection changes at $c = C_1, \ldots, C_n$. More formally, $P \cap \Pi_{C_i - \delta} \neq P \cap \Pi_{C_i + \delta}, \forall i = 1, \ldots, n$, where δ is an arbitrarily small quantity. Then, $C_i(P) = P \cap \Pi_{c_i}$ is called a *cut* of P and $S_i(P) = P \cap \Pi_{C_s}$, for any C_s such that $C_i < C_s < C_{i+1}$, is called a *section* of P. Figure 4 shows an OP with its *cuts* and *sections* perpendicular to the X axis. Since we work with bounded regions, $S_0(P) = \emptyset$ and $S_n(P) = \emptyset$, where n is the total number of *cuts* along a given coordinate axis.

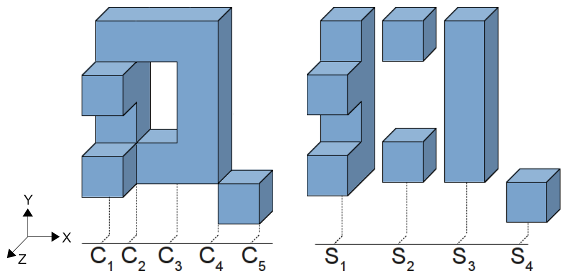

Figure 4: Left: an orthogonal polyhedron with 5 cuts. Right: its sequence of 4 prisms with the representative sections (X direction).

An OP can be represented with a sequence of orthogonal prisms represented by their section. Moreover, if we apply the same reasoning to the representative section of each prism, an OP can be represented as a sequence of boxes. CUDB represents an OP with such an ordered sequence of boxes in a compact way, as many boxes generated by the aforementioned split process are merged into one in several parts of the model. CUDB is axis-aligned like octrees and bintrees, but the partition is done along the object geometry as in binary space partitioning (BSP). Depending on the order of the axes along which we choose to split the data, an object can be decomposed into six different sets of boxes: XYZ, XZY, YXZ, YZX, ZXY, ZYX, and the set will be ordered according to the chosen configuration. Figure 5 illustrates two possible decompositions of the model in Figure 4 (left).

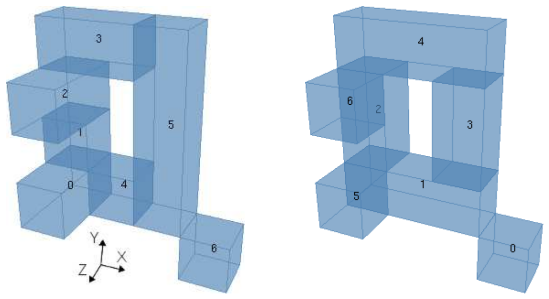

Figure 5: XYZ-CUDB (left) and ZYX-CUDB (right) representation for the model in Figure 4, both with 7 boxes.

In the CUDB model, the adjacency information (either 6 or 26-adjacency) of the boxes is stored. Each box has neighboring boxes in only two orthogonal directions, i.e., for a given *ABC*-ordering, a box can have neighbors only in *A* and *B* direction, and each direction goes in two opposite ways. Thus, there are 4 arrays (2 for each direction) of pointers to the neighboring boxes. For more details of this model see (Cruz-Matías and Ayala, 2011) and (Rodríguez et al., 2011).

4 CONNECTIVITY COMPUTATION

The approach followed in this paper to compute the Euler characteristic and the genus is based on Expression 1, and considers a box as a rectangular prism enclosing a finite number of voxels. In the voxel model, a simple way to compute the number of faces, edges and vertices reported for each voxel when Expression 1 is used, is by checking the lower 13 neighbors (N^-) of the voxel for a backward scan, where the 6 faces, 12 edges and 8 vertices of each visited voxel are added and the possible shared elements (3 faces, 9 edges and 7 vertices) are subtracted. An analogy to this reasoning is used in our approach.

Let β be a box in the CUDB model, β is represented by two diagonally opposed vertices $\vec{v}_0$ and $\vec{v}_1$, the ones with lesser and greater coordinate values respectively, where $\vec{d} = \vec{v}_1 - \vec{v}_0 = (d_x, d_y, d_z)$ represents the main diagonal vector of β and d_x, d_y and d_z its dimensions. Then, for any box β in the CUDB model, the number of enclosed voxels (γ_β), faces (f_β), edges (e_β) and vertices (v_β) are computed as:

$$\gamma_\beta = d_x \cdot d_y \cdot d_z \quad (4)$$

$$f_\beta = [d_x \cdot d_y \cdot (d_z+1)] + [d_x \cdot (d_y+1) \cdot d_z] + [(d_x+1) \cdot d_y \cdot d_z] \quad (5)$$

$$e_\beta = [d_x \cdot (d_y+1) \cdot (d_z+1)] + [(d_x+1) \cdot d_y \cdot (d_z+1)] + [(d_x+1) \cdot (d_y+1) \cdot d_z] \quad (6)$$

$$v_\beta = (d_x+1) \cdot (d_y+1) \cdot (d_z+1) \quad (7)$$

After computing the enclosed unitary elements of β, we have to analyze its backward neighbors (BN), in order to subtract the elements reported by the overlapping regions. For simplicity we consider the XYZ-ordering, therefore, as we said in Section 3, a box can have neighbors only in X and Y direction, so, just the BN in this directions need to be checked.

At this point it is important to say that, independently of the used adjacency pair, (26, 6) or (6, 26), in the binary volume model, our method requires the CUDB with the neighboring boxes information according to 26-adjacency. This is because if we consider a CUDB with 6-adjacency, the connected components still have boxes with overlapping regions that are 26-adjacent, which must be considered in the elements subtraction (e.g. see the boxes 1 and 4 in Figure 5 (left)). Therefore, in order to compute χ and genus for a (6, 26) binary volume model, we simply obtain the connected components of the foreground according to 6-adjacency and then, each of them is separately analyzed with 26-adjacency to count the enclosed elements. For now on we suppose the case of the (26, 6) adjacency pair.

In CUDB when considering 26-adjacency, it is important to notice that two edge-adjacent boxes β_i and β_k are neighbors only in one direction, i.e. if the overlapping region between β_i and β_k is a segment (part of an edge), when it is Y or Z-aligned, β_i and β_k are neighbors in X-direction, and when the segment is X-aligned, β_i and β_k are neighbors in Y-direction. If the overlapping region between β_i and β_k is a vertex, then they are neighbors just in X-direction. For example, in the configurations depicted in Figure 2 (middle and right), the boxes are neighbors in X-direction in both cases.

The method performs a traversal of CUDB and for each box B, computes its unitary elements (γ_β, f_β, e_β, v_β) according to Expressions 4 to 7. However, there are overlapping regions among boxes and the method must deal correctly with them.

4.1 Shared Elements Computation

Overlapping regions can be rectangles (2D), line segments (1D) (segments from now on) or points (0D). They have to be detected and their contribution computed and added or subtracted to the global value.

A box β_i shares a rectangle R with any backward neighbor in X (X-BN) and in Y-direction (Y-BN) (see Figure 6(a) and (b) in red). The basic unitary elements enclosed by this rectangle are computed twice and therefore we have to subtract them once. Let r_x and r_y be the dimensions of R, the faces (f_R), edges (e_R) and vertices (v_R) can be be computed in a way similar to that of Expressions 5 to 7:

$$f_R = r_x \cdot r_y \quad (8)$$

$$e_R = r_x \cdot (r_y+1) + (r_x+1) \cdot r_y \quad (9)$$

$$v_R = (r_x+1) \cdot (r_y+1) \quad (10)$$

However, more than one BN can share a segment with β_i. We have performed an exhaustive case study of the overlapping regions by analyzing the possible neighborings among boxes in the CUDB model. There can be 1, 2 or 3 backward neighboring boxes that share a segment with β_i.

In the first case only the shared rectangle must be computed and subtracted as discussed above. Note that in some cases a degenerated rectangle is obtained (see boxes β_i and β_x in Figure 6(d)).

In the case of two BN of β_i sharing a segment S, it has been subtracted twice and therefore it must be added again. For example, in Figure 6(c) the red regions computed when analyzing the pairs of boxes (β_i, β_x) and (β_i, β_t) have been subtracted and therefore the yellow region has been subtracted twice and has to be added again. There are 4 possible configurations for two BN of β_i sharing a segment.

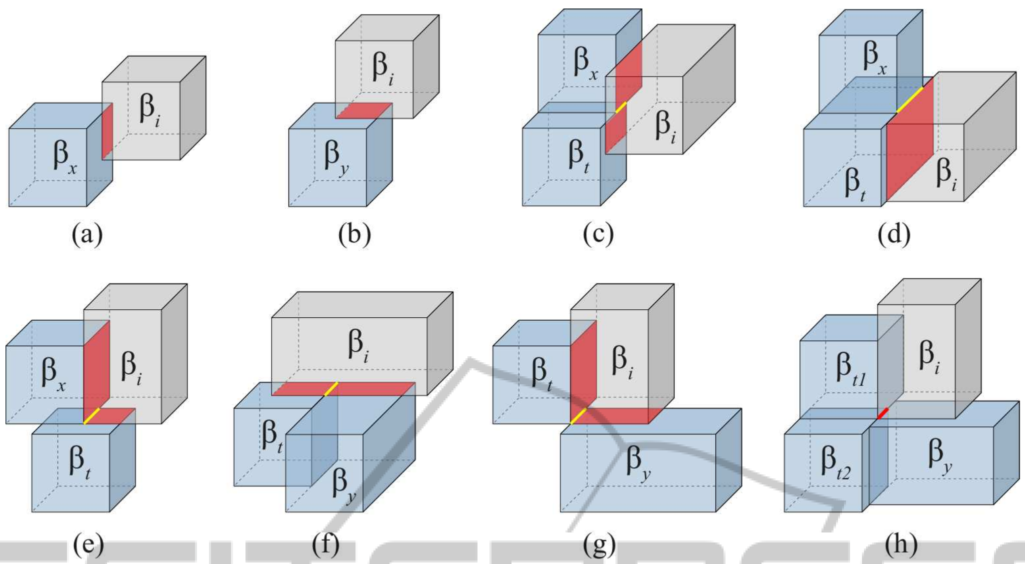

Figure 6: Backward neighbors(BN) configurations of a box β_i. (a) A X-BN sharing a rectangle. (b) A Y-BN sharing a rectangle. (c) Two X-BN sharing a segment. (d) degenerated case of (c). (e) A X and a Y-BN sharing a segment. (f) Two Y-BN sharing a segment. (g) A Y and a X-BN sharing a segment. (h) A Y and two X-BN sharing a segment.

C1. Two X-BN (β_x and β_t), where β_t is Y-BN of β_x. See Figure 6(c and d).

C2. One X-BN (β_x) and one Y-BN (β_t), where β_t is Y-BN of β_x. See Figures 6(e).

C3. Two Y-BN (β_y and β_t), where β_t is X-BN of β_y. See Figure 6(f).

C4. One Y-BN (β_y) and one X-BN (β_t), where β_t is X-BN of β_y. See Figure 6(g).

Then, if s is the length of S, the enclosed unitary edges (e_S) and vertices (v_S) of S are computed as:

$$e_S = s, \qquad v_S = s+1 \tag{11}$$

In the case of three BN of β_i sharing a segment S, there is only one possible configuration:

C5. One Y-BN (β_y) and two X-BN (β_{t1} and β_{t2}), where both β_{t1} and β_{t2} are X-BN of β_y and Y-neighbors between them. See Figure 6(h).

Note that configuration C5 is equivalent to two occurrences of C1 ($(\beta_y, \beta_{t1}, \beta_{t2})$ and $(\beta_i, \beta_{t1}, \beta_{t2})$) and two occurrences of C4 ($(\beta_i, \beta_y, \beta_{t1})$ and $(\beta_i, \beta_y, \beta_{t2})$). However, both configurations C4 occur when β_i is being analyzed and, therefore, some shared elements with β_{t1} in one occurrence and with β_{t2} in the other, are added twice, so, the shared segment S by β_i, β_{t1} and β_{t2} (highlighted in red in Figure 6(h)), represents the region that must be re-subtracted. The enclosed unitary edges (e_S) and vertices (v_S) are computed as in Expression 11. This case is solved by inserting all the β_t of configurations C4 into a list and then the list is analyzed in order to check for boxes that are Y-BN.

4.2 Connected Component Labeling

For the CCL process, we have followed the classical two-pass strategy of first labeling and then renumbering a set of equivalences (Wu et al., 2009). As we have the neighbors of each box, we avoid the neighborhood test. In our labeling process the CUDB model is traversed and, on the fly, each box β_i is labeled with the minimum value of its already labeled BN, or with a new label if it doesn't have labeled BN. When β_i has two or more labeled BN with different values, a label equivalence is recorded into a map, where the key value corresponds to the region number and the mapped value to its label. All the equivalences are solved in the renumbering pass that first sorts out all the equivalences and then propagates them correctly. As a result, we get the number of connected components.

As both the connectivity computation and the CCL processes require a traversal of the boxes and its BN, we have merged both algorithms into one. The proposed method uses the CUDB representation (CUDB-Rep) of an OP that has already been computed. The next pseudo-code represents the whole process.

Input: CUDB-Rep of the OP.
Output: Euler characteristic (χ) and genus.

```
1. $currentLabel = n_0 = n_1 = n_2 = n_3 = 0$.
2. For each box, $\beta_i, i = 1..n$, in the CUDB-Rep do:
   A. Compute $\gamma_i$, $f_i$, $e_i$, $v_i$.
```

```
  B. Do $mlabel = \infty$.
  C. for each X-BN $\beta_x$ do:
     i. if $\beta_x.label < mlabel$ then, $mlabel = \beta_x.label$
     ii. Compute $f_R$, $e_R$ and $v_R$.
     iii. Do $f_i$–=$f_R$, $e_i$–=$e_R$ and $v_i$–=$v_R s$.
     iv. for each X-BN, $\beta_t$ do: //Configurations C1
         (a) if $\beta_t$ is Y-BN of $\beta_x$, then, compute $e_S$ and
             $v_S$, and do $e_i$+=$e_S$ and $v_i$+=$v_S$.
     v. for each Y-BN, $\beta_t$ do: //Configurations C2
         (a) if $\beta_t$ is Y-BN of $\beta_x$, then, compute $e_S$ and
             $v_S$, and do $e_i$+=$e_S$ and $v_i$+=$v_S$.
  D. for each Y-BN, $\beta_y$ do:
     i. if $\beta_y.label < mlabel$ then, $mlabel = \beta_y.label$
     ii. Compute $f_R$, $e_R$ and $v_R$.
     iii. Do $f_i$–=$f_R$, $e_i$–=$e_R$ and $v_i$–=$v_R$.
     iv. for each Y-BN, $\beta_t$ do: //Configurations C3
         (a) if $\beta_t$ is X-BN of $\beta_y$, then, compute $e_S$
             and $v_S$, and do $e_i$+=$e_S$ and $v_i$+=$v_S$.
     v. Create a list of boxes $L$.
     vi. for each X-BN, $\beta_t$ do: //Configurations C4
         (a) if $\beta_t$ is X-BN of $\beta_y$, then, compute $e_S$
             and $v_S$, do $e_i$+=$e_S$ and $v_i$+=$v_S$ and insert
             $\beta_t$ to $L$.
     vii. for each pair ($\beta_{t1}$ , $\beta_{t2}$) in $L$ which are Y-
          neighbors do: //Configurations C5
         (a) Compute $e_S$ and $v_S$.
         (b) Do $e_i$–=$e_S$ and $v_i$–=$v_S$.
  E. Do $n_0$+=$v_i$, $n_1$+=$e_i$, $n_2$+=$f_i$, and $n_3$+=$\gamma_i$.
  F. if $mlabel = \infty$ then
     i. Do $mlabel = currentLabel$.
     ii. Do $currentLabel$++.
  G. for each X-BN and Y-BN, $\beta_t$ do:
     i. if $\beta_t$ is labeled, then, add equivalence
        $\beta_t.label$ = $mlabel$ into the map equivalences.
     ii. else do $\beta_t$.label= $mlabel$.
3. Do $\chi = n_0 - n_1 + n_2 - n_3$.
4. Number of cc ($h_0$) = renumbering(equivalences).
5. Compute the complement of CUDB-Rep.
6. Number of cavities ($h_2$) = CCL(complement)-1.
7. Do $genus(h_1) = h_0 + h_2 - \chi$.
```

Step 2 computes the same number of voxels, faces, edges and vertices that the voxel-based method and simultaneously performs the first step of the CCL process. Step 3 computes χ using Expression 1. Step 4 performs the CCL relabeling process, which returns the number of connected components. Step 6 applies our standard version of CUDB-based CCL to compute the number of internal cavities (the connected components of the object complement). Finally, step 7 computes the genus using Expression 3.

5 RESULTS

We have measured χ and the genus for a selection of datasets with different shape features and size. They present non-manifold configurations and may contain isolated cavities and disconnected components. Figure 7 shows rendered views of the test datasets and its size in the voxel model, where from (j) to (r) are real volume data coming from CT or MRI scanners. These datasets come from public volume repositories. Three methods have been compared: voxel-based, OP-based (see Section 2) and CUDB-based, presented in this paper. These methods produce exactly the same results. The algorithms has been written in C++ and tested on a PC Intel®Core 2 E6600 at 2.4 GHz with 3.2 Gb RAM under Linux.

We work on a platform where the main representation models are CUDB and the Extreme Vertices Model (EVM), which is a very concise B-Rep model for OP with very fast Boolean operations. EVM can be obtained from the voxel model, in turn, CUDB is obtained from EVM. The conversions algorithms have been published (Aguilera, 1998; Cruz-Matías and Ayala, 2011). These models are used in other processes in diverse research topics, so, we consider that they are available and ignore the cost of conversion from the voxel model, similar to the OP-based method. Thus, to compute the complement of the input model, we use the EVM representation, whose runtime is negligible. However, the conversion time of the complement to CUDB is considered in our computation times (step 5 of the algorithm).

Table 1 shows the attributes of the tested datasets: number of foreground voxels, number of boxes in their CUDB-Rep, number of connected components (C^+), number of isolated cavities (C^-), χ and genus using the adjacency pair (26, 6).

Table 2 shows the required time in seconds to compute χ and the genus for each referenced method. To compute the genus, the three methods need to compute the complement of the model, and besides, the OP-based method needs to convert the OP to a homotopic manifold analog. Note that our proposal is very fast to compute χ, and regarding the genus computation, it is by far, faster than the voxel-based method, in some datasets up to two orders of magnitude (pelvis, golfBall, pegasus, aneurysm and beetle). Compared to the previous OP-based our method is also faster in all the tested datasets, in some of them up to an order of magnitude (pegasus, teddy and femur). Moreover, we report the conversion times: voxel to EVM (tc_1) and EVM to CUDB (tc_2) in order to show that, even considering these costs, the overall time (t_o) of our method is better than the voxel-based method.

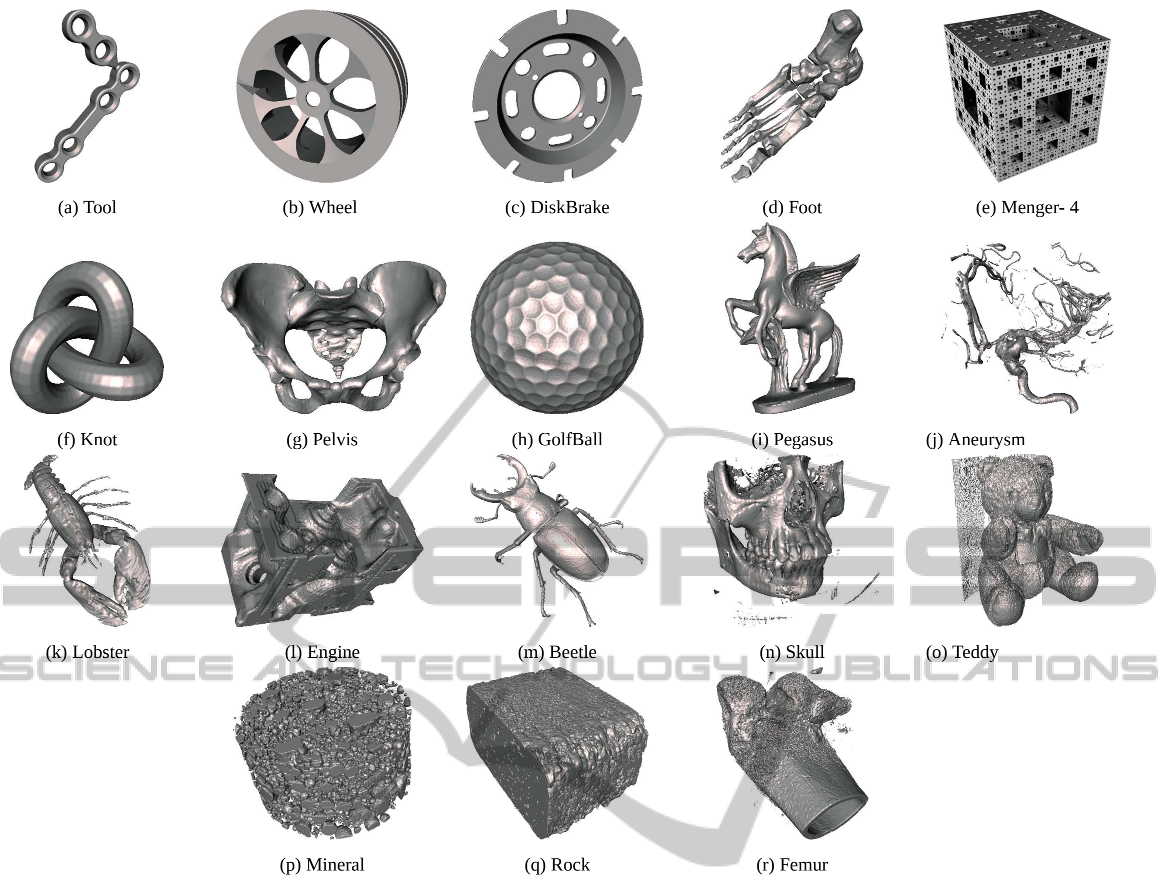

Figure 7: Rendered images of the test datasets.

Table 1: Attributes of the test datasets. For each dataset, the size of the voxel model, number of foreground voxels, number of boxes in its CUDB-Rep. Next, with an adjacency pair (26,6): the number of connected components, number of isolated cavities, the Euler characteristic χ and genus.

Dataset	size	# for. vox.	# boxes	C^+	C^-	χ	genus
(a) Tool	511x339x48	1778611	11000	1	0	-10	6
(b) Wheel	120x300x300	3809958	13207	1	0	-14	8
(c) DiskBrake	511x512x73	2584762	29516	1	0	-20	11
(d) Foot	183x512x185	1818019	35498	6	24	-86	73
(e) Menger-4	162x162x162	1280000	46704	1	0	-52864	26433
(f) Knot	329x350x257	7509337	76831	1	0	0	1
(g) Pelvis	368x512x450	5920950	85923	1	8	-10	14
(h) GolfBall	510x509x511	13645424	129493	1	0	2	0
(i) Pegasus	598x800x574	24683709	191747	1	8	2	8
(j) Aneurysm	213x215x240	69743	10705	406	12	544	146
(k) Lobster	244x239x49	233509	19322	53	180	-638	552
(l) Engine	139x197x108	901818	25524	9	194	146	130
(m) Beetle	411x371x247	1737343	36052	17	114	-190	226
(n) Skull	256x256x256	1112906	114563	1624	337	-1020	2471
(o) Teddy	424x321x493	24758866	124063	59	212	-2580	1561
(p) Mineral	376x375x206	7363953	232008	724	5	-2792	2125
(q) Rock	240x406x267	19348939	331491	1336	17263	25828	5685
(r) Femur	463x494x628	4014089	838585	22714	7909	-25144	43195

Table 2: Statistics of the test dataset. For each dataset the computation time in seconds for the voxel-based (mvx), OP-based and the CUDB-based methods. The last columns represent the conversion times: voxel to EVM (tc_1) and EVM to CUDB (tc_2) of the original model, $t_o = tc_1 + tc_2 + CUDB^*$.

Dataset	Time χ			Total time (genus)			tc_1	tc_2	t_o
	mvx	*OP*	*CUDB*	*mvx*	*OP*	$CUDB^*$			
(a) Tool	1.77	0.26	**0.01**	6.22	0.84	**0.11**	1.47	0.13	*1.71*
(b) Wheel	3.84	0.24	**0.01**	10.84	1.47	**0.20**	2.60	0.20	*3.00*
(c) DiskBrake	4.94	0.81	**0.01**	17.09	2.42	**0.28**	5.24	0.22	*5.73*
(d) Foot	7.72	0.79	**0.02**	22.22	2.45	**0.29**	4.58	0.25	*5.13*
(e) Menger-4	1.30	0.70	**0.02**	3.85	1.52	**0.27**	1.05	0.21	*1.53*
(f) Knot	9.19	1.94	**0.05**	29.07	5.83	**0.64**	1.94	0.49	*3.06*
(g) Pelvis	26.81	2.16	**0.06**	101.21	6.93	**0.71**	23.33	0.55	*24.59*
(h) GolfBall	41.53	2.90	**0.07**	150.37	9.49	**1.20**	34.72	0.89	*36.81*
(i) Pegasus	71.54	6.15	**0.13**	274.83	20.81	**1.88**	72.82	1.46	*76.16*
(j) Aneurysm	2.99	0.37	**0.01**	10.26	0.92	**0.10**	2.57	0.08	*2.75*
(k) Lobster	0.61	0.49	**0.02**	2.14	1.31	**0.16**	0.63	0.13	*0.92*
(l) Engine	0.77	0.62	**0.02**	2.43	1.77	**0.21**	0.71	0.16	*1.07*
(m) Beetle	11.08	2.01	**0.02**	39.39	2.34	**0.29**	9.49	0.25	*10.03*
(n) Skull	5.74	3.51	**0.06**	19.40	9.16	**0.94**	5.10	0.68	*6.71*
(o) Teddy	20.97	3.49	**0.09**	74.07	10.39	**1.02**	18.23	0.77	*20.01*
(p) Mineral	9.35	5.92	**0.16**	31.04	19.25	**1.97**	8.76	1.48	*12.22*
(q) Rock	12.48	9.47	**0.39**	33.89	24.43	**3.44**	8.65	1.93	*14.01*
(r) Femur	45.94	31.16	**0.80**	170.64	80.66	**8.06**	41.90	5.69	*55.65*

6 CONCLUSIONS AND FUTURE WORK

We have presented a method to compute the Euler characteristic and the genus of binary volume datasets using the CUDB model, and we have evaluated its performance compared to existing methods applied to voxel models and OP. We have tested several public volume datasets, both phantom and real. We conclude that computing the connectivity is notably faster in our approach. The performance variability is caused by the dataset size but above all to their surface intricacy: the voxel-based method performance is function of the number of voxels, but our method depends on the number of boxes, tightly related to the model's tortuosity (a property that represents the twist of a curve, i.e. the degree of turns or detours a model has (Grisan et al., 2003)), like the previous developed methods based on OP.

As future work, we plan to study a method to compute the complement of a model directly from its CUDB-Rep, in order to leave aside the EVM representation, since, as can be seen in Table 2, the difference in time to compute χ and genus is mainly due to the conversion of the complement from EVM to CUDB. Furthermore, in the biomedical field, there are other structural parameters that can be studied to describe properties of a biomaterial, in this field we have used the CUDB model in a method to simulate the mercury intrusion in a porous medium (Rodríguez et al., 2011). At present, we are beginning to study simplification (Cruz-Matías and Ayala, 2012) and time-varying techniques based on EVM and CUDB models.

ACKNOWLEDGEMENTS

This work was partially supported by the national projects TIN2008-02903 and TIN2011-24220 and a MAEC-AECID grant for I. Cruz-Matías, all of the Spanish government. The authors thank the anonymous reviewers whose remarks and suggestions have allowed to greatly improve the paper.

REFERENCES

Aguilera, A. (1998). *Orthogonal Polyhedra: Study and Application.* PhD thesis, LSI-UPC.

Andújar, C., Brunet, P., and Ayala, D. (2002). Topology-reducing surface simplification using a discrete solid rep. *ACM Trans. on Graphics*, 21(2):88 – 105.

Ayala, D., Vergés, E., and Cruz, I. (2012). A polyhedral approach to compute the genus of a volume dataset. In *Proceedings of the GRAPP 2012*, pages 38–47, Rome, Italy. INSTICC Press.

Cruz-Matías, I. and Ayala, D. (2011). CUDB: An improved decomposition model for orthogonal pseudo-polyhedra. Technical Report LSI-11-2-T, UPC.

Cruz-Matías, I. and Ayala, D. (2012). Orthogonal simplification of objects represented by the extreme vertices model. In *Proceedings of the GRAPP 2012*, pages 193–196, Rome, Italy. INSTICC Press.

Dillencourt, M., Samet, H., and Tamminen, M. (1992). A general approach to connected-component labeling for arbitrary image representations. *Journal of the ACM*, 39(2):253 – 280.

Grevera, G. J., Udupa, J. K., and Odhner, D. (2000). An order of magnitude faster isosurface rendering in software on a PC than using dedicated, GP rendering hardware. *IEEE Trans. Vis. and CG.*, 6(4):335–345.

Grisan, E., Foracchia, M., and Ruggeri, A. (2003). A novel method for the automatic evaluation of retinal vessel tortuosity. In *Proc. of the 25th Annual Int. Conf. of the IEEE EMBS, 2003.*, volume 1, pages 866 – 869 Vol.1.

Khachan, M., Chenin, P., and Deddi, H. (2000). Polyhedral representation and adjacency graph in n-dimensional digital images. *Computer Vision and Image understanding*, 79:428 – 441.

Kim, B., Seo, J., and Shin, Y. (2001). Binary volume rendering using Slice-based Binary Shell. *The Visual Computer*, 17:243 – 257.

Kong, T. and Rosenfeld, A. (1989). Digital topology: Introduction and survey. *Computer Vision, Graphics and Image Processing*, 48:357–393.

Konkle, S., Moran, P., Hamann, B., and Joy, K. (2003). Fast methods for computing isosurface topology with Betti numbers. In *Data Visualization*, pages 363 – 376.

Lachaud, J. and Montanvert, A. (2000). Continuous analogs of digital boundaries: A topological approach to isosurfaces. *Graphical Models*, 62:129 – 164.

Latecki, L. (1997). 3D Well-Composed Pictures. *Graphical Models and Image Processing*, 59(3):164–172.

Latecki, L., Eckhardt, U., and Rosenfeld, A. (1995). Well-composed sets. *Computer Vision and Image Understanding*, 61(1):70–83.

Mantyla, M. (1988). *An Introduction to Solid Modeling*. Computer Science Press.

Martín-Badosa, E., Elmoutaouakkil, A., Nuzzo, S., Amblard, D., Vico, L., and Peyrin, F. (2003). A method for the automatic characterization of bone architecture in 3D mice microtomographic images. *Computerized Medical Imaging and Graphics*, 27:447–458.

Massey, W. S. (1991). *A Basic Course in Algebraic Topology*. Springer-Verlag.

Odgaard, A. and Gundersen, H. J. (1993). Quantification of Connectivity in Cancellous Bone, with Special Emphasis on 3-D Reconstructions. *Bone*, 14:173 – 182.

Rodríguez, J., Cruz, I., Vergés, E., and Ayala, D. (2011). A connected-component-labeling-based approach to virtual porosimetry. *Graphical Models*, 73:296–310.

Samet, H. (1990). *Applications of spatial data structures: Computer graphics, image processing, and GIS*. Addison-Wesley Longman Publishing Co., Inc.

Schaefer, S., Ju, T., and Warren, J. (2007). Manifold dual contouring. *IEEE Transactions on Visualization and Computer Graphics*, 13(3):610 – 619.

Toriwaki, J. and Yonekura, T. (2002). Euler number and connectivity indexes of a three dimensional digital picture. *Forma*, 17:183–209.

Vanderhyde, J. and Szymczak, A. (2008). Topological simplification of isosurfaces in volume data using octrees. *Graphical Models*, 70:16 – 31.

Vogel, H. J., Tölke, J., Schulz, V., Krafczyk, M., and Roth, K. (2005). Comparison of a lattice-boltzmann model, a full-morphology model, and a pore network model for determining capillary pressure-saturation relationships. *Vadose Zone Journal*, 4:380 –388.

Wu, K., Otoo, E., and Suzuki, K. (2009). Optimizing two-pass connected-component labeling algorithms. *Pattern Anal. Appl.*, 12(2):117–135.